31st Congress of the International Council of the Aeronautical Sciences

Belo Horizonte, Brazil; September 09-14, 2018

ROBUST TRAJECTORY OPTIMIZATION OF VTOL TRANSITION MANEUVER USING BI-LEVEL OPTIMAL CONTROL

Patrick Piprek* **and Florian Holzapfel***

* **Technical University of Munich, Institute of Flight System Dynamics, Bolzmannstrasse 15, 85748 Garching bei Muenchen, Germany**

Keywords: *generalized polynomial chaos, direct optimal control, robust trajectory optimization, bi-level optimal control, VTOL aircraft*

Abstract

This study deals with the robust optimization of the transition maneuver for a vertical take-off and landing drone (VTOL) using a bi-level optimal control (OC) approach: The upper level, parameter optimization, problem is optimized using a differential evolution (DE) genetic algorithm. By this a global optimal solution is achieved.

On the other hand, the lower level problem is solved by using a gradient-based direct OC scheme. The distinctiveness of this lower level setup is the fact that not only the general mean optimization problem is solved, but an OC problem (OCP) with uncertainties. This combination yields the possibility to calculate robust trajectories.

The uncertainty modeling is done by means of generalized polynomial chaos (gPC). Thus, the lower level problems are not only solved at one specific set of parameters, but on multiple parameter sets to calculate the uncertainty influence on the optimal trajectory in distinct parameters.

The developed algorithm is applied to the transition maneuver, including the climb to a safe altitude, of a VTOL. The results show an enhancement of the optimal trajectory in the sense of robustness with respect to wind influences regarding the safety of the transition maneuver.

1 Introduction

Optimization plays an integral part in today's engineering applications. Especially in aircraft related topics, where there are both intense competition as well as expensive resources and hard constraints (e.g., noise emission), the role of optimization is crucial.

Up until now, many studies concerned with optimization either did not consider uncertainties at all or did so in a very limited manner [1, 2]. Thus, the goal of this study is to show a methodology for robust OC using a bi-level framework. The case study is the transition maneuver (including safe altitude climb) of a VTOL.

Original studies on OC of aircraft with uncertainties did combine the gPC method [3] as a wrapper around the OC framework [4, 5]. Thus, these methods did not calculate robust trajectories in the sense of this study (i.e., that the calculated trajectory is least sensitive to the uncertainties), but mainly calculated an uncertain representation of the trajectory.

More recent studies in the field of conflict resolution [6], short-time climb of supersonic aircraft [7], and flight in severe weather conditions [8] still use the gPC method, but now try to find an incorporation of the gPC expansion within the OC discretization. Thus, these studies are more related to the developed framework of this study.

Another approach, used for the calculation of noise minimal trajectories uses a bi-level OC framework [9]. By this approach, the calculation of robust trajectories is split up in two levels, a parameter optimization and a dynamic model optimization level, and afterwards linked by a parameter dependency between the two levels.
Within this study, we also develop a bi-level OC framework and extend the methods developed in [9] by using control effectiveness parameters as optimization variables of the upper level. Additionally, the upper level is solved using a DE algorithm.
Therefore, the study is organized as follows: The gPC method is introduced in section 2. Section 3 introduces the bi-level OC framework that is proposed within this study and used to calculate robust optimal trajectories. The test results are introduced in section 4 and section 5 concludes the study with an outlook and perspectives.

2 Generalized Polynomial Chaos

The gPC method was developed by XIU and KARNIADAKIS in [3] and is an extension of the work of NORBERT WIENER on Gaussian uncertainties [10]. The next subsections introduce the general definition of gPC (subsection 2.1), the stochastic collocation (SC) method that is used to sample the gPC expansion (subsection 2.2), and the calculation of the statistical moments (subsection 2.3). Overall, the gPC method is the baseline formulation of the lower level of the bi-level OCP as introduced in section 3. In the end, the statistical moment calculation of subsection 2.3 is utilized to shape a robust trajectory.

2.1 Definition

The gPC method is defined by a finite sum expansion with deterministic expansion coefficients $\hat{\mathbf{y}} \in \mathbb{R}^{n_y \times M}$ and orthonormal polynomials (normalized orthogonal polynomials) $\Phi \in \mathbb{R}^{M \times 1}$ related to the uncertainties to approximate the system outputs $\mathbf{y} \in \mathbb{R}^{n_y \times 1}$ as follows [11]:

$$\mathbf{y}(\mathbf{z};\theta) \approx \sum_{m=0}^{M-1} \hat{\mathbf{y}}_m(\mathbf{z})\,\Phi_m(\theta) \tag{1}$$

Here, the orthonormal polynomials are chosen with respect to the probability distribution ρ of the uncertain parameters $\theta \in \mathbb{R}^{n_\theta \times 1}$ (Table 1).
The deterministic parameters are summarized within the vector $\mathbf{z} \in \mathbb{R}^{n_z \times 1}$ (including system states $\mathbf{x} \in \mathbb{R}^{n_x \times 1}$ and controls $\mathbf{u} \in \mathbb{R}^{n_u \times 1}$ respectively). The expansion coefficients are calculated using a Galerkin projection as follows [11]:

$$\hat{\mathbf{y}}_m(\mathbf{z}) = \int_\Omega \mathbf{y}(\mathbf{z};\theta)\,\Phi_m(\theta)\,\rho(\theta)\mathrm{d}\theta \tag{2}$$

It is evident that Eq. 2 is not straightforward to solve as the expansion coefficients are themselves depending on the system response.
Thus, subsection 2.2 introduces the SC method that employs a Gaussian quadrature [12] and deterministic sampling to evaluate the integral in Eq. 2.

2.2 Stochastic Collocation

Using the SC method, the integral in Eq. 2 gets expanded into a Gaussian quadrature sum as follows [11]:

$$\hat{\mathbf{y}}_m(\mathbf{z}) = \sum_{j=1}^{Q} \mathbf{y}\left(\mathbf{z};\theta^{(j)}\right)\Phi_m\left(\theta^{(j)}\right)\alpha\left(\theta^{(j)}\right) \tag{3}$$

Here, $\theta^{(j)}$ and $\alpha\left(\theta^{(j)}\right)$ are the expansion nodes and expansion weights respectively. These are, again, determined by the orthonormal polynomials and their corresponding probability distribution (Table 1) [12].
Therefore, the problem of calculating the integral in Eq. 2 reduces to a deterministic sampling at the expansion nodes and subsequent evaluation of Eq. 3. Consequently, the OCP must be solved at each expansion node.

2.3 Statistical Moments

Statistics are obtained fairly easy from the gPC expansion formula in Eq. 1 by using the basic definition for statistical moments as follows [12]:

$$\mathbb{E}\left[\theta^k\right] = \int_\Omega \theta^k \rho(\theta)\,\mathrm{d}\theta \tag{4}$$

Table 1: Continuous probability distribution - orthogonal polynomial connection within the Wiener-Askey scheme (after [11])

Probability Distribution	Weight Function ρ	Support Ω	Symbol	Orthogonal Polynomial
Gaussian/Normal	$\frac{1}{\sqrt{2\pi}}\exp\left(\frac{\theta^2}{2}\right)$	$]-\infty,\infty[$	$N(\mu,\sigma)$	Hermite
Gamma	$\frac{\theta^{\alpha}\exp(-\theta)}{\Gamma(\alpha+1)}$	$[0,\infty[$	$\gamma(\mu,\sigma,\alpha)$	Laguerre
Beta	$\frac{\Gamma(\alpha+\beta+2)}{2^{\alpha+\beta+1}\Gamma(\alpha+1)\Gamma(\beta+1)}(1-\theta)^{\alpha}(1+\theta)^{\beta}$	$]-1,1[$	$B(a,b,\alpha,\beta)$	Jacobi
Uniform	$\frac{1}{2}$	$]-1,1[$	$U(a,b)$	Legendre

For instance, the mean μ ($k=0$ in Eq. 4) and standard deviation σ (the square root of the variance with $k=1$ in Eq. 4 and centered around the mean value) are only dependent on the expansion coefficients themselves and given by [11] as follows:

$$\begin{aligned}\mu[\mathbf{y}(\mathbf{z};\theta)] &\approx \hat{\mathbf{y}}_0(\mathbf{z})\\ \sigma[\mathbf{y}(\mathbf{z};\theta)] &\approx \sqrt{\sum_{m=1}^{M-1}\hat{\mathbf{y}}_m^2(\mathbf{z})}\end{aligned} \tag{5}$$

Higher order statistics can be calculated as well by using Eq. 4, but are no longer independent of the orthonormal polynomials [11].
As mean and standard deviation are used within this study as main indicators of robustness, the statistics given in Eq. 5 are sufficient.

3 Bi-level Framework

This section introduces the bi-level OC framework used in this study to calculate robust trajectories for the transition of a VTOL. The general structure of the framework is depicted in Figure 1.
It is illustrated that the lower level (subsection 3.1) uses the gPC formulation and the SC approach to calculate statistical moments for the optimal trajectories. Gradient-based OC methods are used to calculate the optimal trajectories.
The statistics are then given to the upper level (subsection 3.2) that in turn tries to optimize the uncertainty in the trajectory to be minimal. For this, an optimization based on DE is proposed. The upper level ultimately enforces control authority factors on the lower level that shape the trajectory by changing the state dynamics and statistics of the optimal trajectory. It should be noted that the control authority factors are constant along the trajectory. Therefore, a trade-off for the whole trajectory is sought.
The overall optimization procedure is summarized as follows: The upper level problem optimizes the parameters $k_1,\ldots,k_m$ that are control effectiveness parameters in this study and are therefore directly able to shape the trajectory. These parameters are assigned to the lower level OCP that is evaluated with these upper level control effectiveness parameters to a gPC expansion. This yields the response of the aircraft to uncertain parameters. Finally, these responses are used to calculate the moments of the uncertain trajectory (e.g., mean and standard deviation) that are then again fed to the upper level problem and its cost functional. This cost functional is e.g., the minimization of the standard deviation or sensitivity of the optimized trajectory.
Overall, this procedure leads to a robust trajectory, as the optimized trajectory is then subject to a minimized uncertainty influence based on the upper level cost function.
The developed robust bi-level OC structure is examined in a case study for the transition maneuver with climb of a VTOL in section 4.

3.1 Lower Level Problem Formulation

As stated in previous paragraphs, the lower level problem in the bi-level OC framework is based on gradient-based OC. The problem formulation

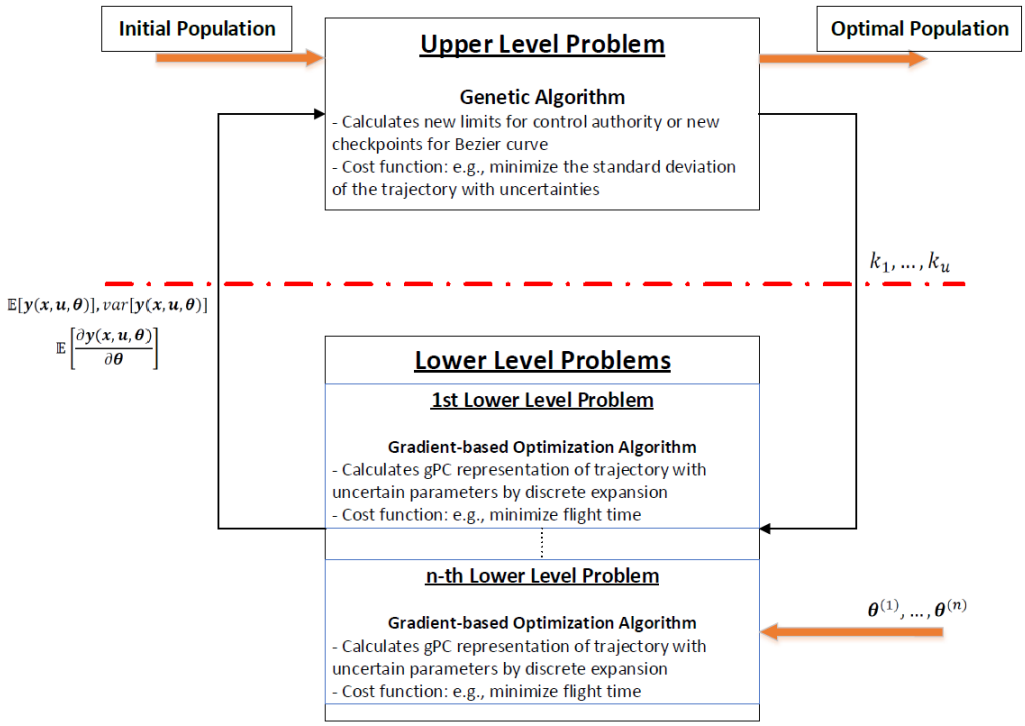

Fig. 1 : Structure of the robust bi-level optimal control framework for the robust trajectory optimization algorithm of this study.

is as follows [13]:

$$\begin{aligned} \min_{\mathbf{z}, t_f} \quad & J = e(\mathbf{z}) + \int_{t_0=0}^{t_f} L(\mathbf{z})\,\mathrm{d}t \\ \text{s.t.} \quad & \mathbf{f}(\mathbf{z};\theta) = \dot{\mathbf{x}}, \\ & \mathbf{c}(\mathbf{z}) \leq \mathbf{0}, \\ & \psi(\mathbf{z}) = \mathbf{0} \end{aligned} \tag{6}$$

The goal is to minimize the cost functional J (described by Mayer e and Lagrange L term) subject to the equality path-/pointconstraints ψ and the inequality path-/pointconstraints $\mathbf{c}$ respectively. Additionally, the state dynamics $\mathbf{f}$ including uncertainties must be fulfilled.
For the transcription of the OCP, the MATLAB-based toolbox FALCON.M [14] is used. The solution of the transcribed OCP is achieved by using the open source optimizer IPOPT [15].
The optimization model is based on a rigid body representation [16] of a VTOL as depicted in Figure 2 (subsection 4.1). The figure also contains the definition of the body-fixed reference frame. The lower level OCP is optimized with respect to

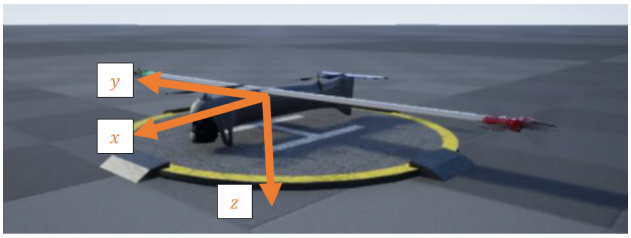

Fig. 2 : View on used VTOL model for the bi-level optimal control of the transition maneuver including body-fixed frame of reference with parameter exchange between the two levels.

a minimal flight time, i.e., $J = t_f$, and evaluated according to the gPC expansion (section 2). The statistics are calculated according to Eq. 5.

3.2 Upper Level Problem Formulation

The upper level problem is a parameter optimization problem with no dynamic model. It uses a DE [17] strategy to optimize the statistics of the lower level problem. The structure of the implemented DE algorithm is given in Figure 3. Take

into account that step 4, i.e., the calculation of the new cost values, is the most time consuming as here the lower level OCP must be solved. But, as they are independent of one another, this part is parallelized fairly easy.
Overall, the upper level tries to find the optimal control authorities that minimize its cost. This cost in turn shapes a robust trajectory by adapting the control authorities as it depends on the uncertain representation of the OC trajectories. This makes it possible to calculate the robust trajectories desired in this study.
It should be noted that after the DE algorithm calculated a suitable optimal parameter set, a further gradient based optimization is conducted with this initial parameter set. This is done to really calculate the optimal parameter set in a local area, while the DE algorithm is consequently used to find the region of the optimal set.

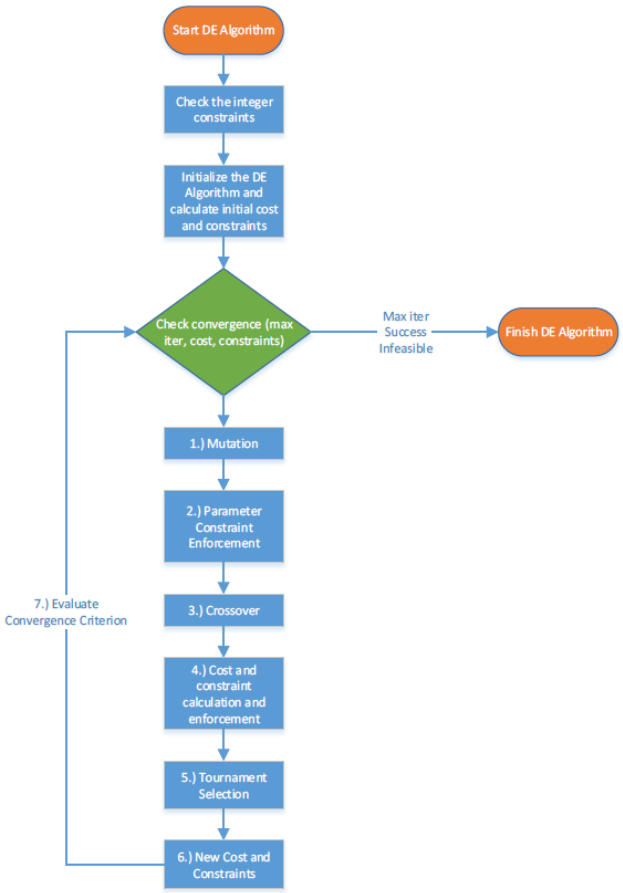

Fig. 3 : Flowchart of differential evolution algorithm used in this study for the optimization of the upper level optimal control problem.

4 Test Case

This section introduces the test case results for the bi-level OC framework. Subsection 4.1 describes the model for the test case with the results given in subsection 4.2. The optimization is based on the transition of a VTOL including an escape from a funnel, i.e., a climb to a safe altitude.

4.1 Optimization Model

The optimization model is based on a rigid body representation of a VTOL on a fixed flat earth environment [16]. The states and controls with their bounds for the OC are listed in Table 2. Additionally, this table also includes the constraint outputs for the OCP.
As it is seen from Table 2, we are using the standard states for a rigid body model of an aircraft including quaternions as the VTOL is also able to climb vertically. The equations of motion are

stated as follows [16]:

$$\begin{bmatrix} \mathbf{E}_3 & \mathbf{0}_{3\times4} & \mathbf{0}_3 & \mathbf{0}_3 \\ \mathbf{0}_{4\times3} & \mathbf{E}_4 & \mathbf{0}_{4\times3} & \mathbf{0}_{4\times3} \\ \mathbf{0}_3 & \mathbf{0}_{3\times4} & m\mathbf{E}_3 & m\mathbf{R}_{CG}^T \\ \mathbf{0}_3 & \mathbf{0}_{3\times4} & m\mathbf{R}_{CG} & \mathbf{I} \end{bmatrix} \dot{\mathbf{x}} = \begin{bmatrix} \mathbf{0}_3 & \mathbf{0}_{3\times4} & \mathbf{P} & \mathbf{0}_3 \\ \mathbf{0}_{4\times3} & \frac{1}{2}\mathbf{O} & \mathbf{0}_{4\times3} & \mathbf{0}_{4\times3} \\ \mathbf{0}_3 & \mathbf{0}_{3\times4} & -\Omega & \mathbf{0}_3 \\ \mathbf{0}_3 & \mathbf{0}_{3\times4} & -m\mathbf{I}^{-1}\mathbf{R}_{CG}\Omega & -\mathbf{I}^{-1}\Omega\mathbf{I} \end{bmatrix} \mathbf{x} + \begin{bmatrix} \mathbf{0}_{3\times1} \\ \mathbf{0}_{4\times1} \\ \frac{1}{m}\left(\mathbf{F} - \Omega\Omega\mathbf{r}_{CG}\right) \\ \mathbf{I}^{-1}\mathbf{M} \end{bmatrix} \tag{7}$$

The identity and zero matrix of appropriate size as given by the index are denoted by $\mathbf{E}$ and $\mathbf{0}$ respectively (if only one index is given the matrix is square). The mass is given by m, the inertia tensor by $\mathbf{I}$. The forces and moments that act on the VTOL (containing aerodynamics, propulsion, and gravitation) are denoted by $\mathbf{F}$ and $\mathbf{M}$ respectively. The aerodynamics and propulsion modules are based on lookup tables, while the gravitation and atmosphere are modeled according to the ISA atmosphere [18].
The distance vector $\mathbf{r}_{CG}$ contains the distance between the equation of motion reference point and the center of gravity with the cross product skew-symmetric matrix given by $\mathbf{R}_{CG}$. This distance relates to a coupling of translation and rotation, and by this longitudinal and lateral plane. This can also be seen in the results in subsection 4.2. The skew-symmetric matrix of the rotation states is denoted by Ω.
Now, the matrix $\mathbf{P}$ is the projection of the velocity on the position propagation for the fixed-flat earth and simply given as follows:

$$\mathbf{P} = \begin{bmatrix} -1 & 0 & 0 \\ 0 & 1 & 0 \\ 0 & 0 & -1 \end{bmatrix} \tag{8}$$

The attitude propagation for the quaternion is given as follows [16]:

$$\mathbf{O} = \begin{bmatrix} 0 & -p & -q & -r \\ p & 0 & r & -q \\ q & -r & 0 & p \\ r & q & -p & 0 \end{bmatrix} \tag{9}$$

After stating the equations of motion, the system outputs (Table 2) containing the funnel distance d_F that enforces the VTOL to climb to a safe altitude are considered. The funnel is hereby defined by using a sigmoid shaped function as follows:

$$s(x,y) = s_{scale} \cdot \frac{\exp\left(\sqrt{x^2+y^2}+s_{off}\right)}{\exp\left(\sqrt{x^2+y^2}+s_{off}\right)+1} + s_{shift} \tag{10}$$

Here, $s_{scale} = 5$, $s_{off} = -2$, and $s_{shift} = -1$ denote the scaling, offset, and shift parameter of the sigmoid function $s(x,y)$ respectively. The funnel distance d_F is consequently the height above the funnel.
The initial and final state bounds for the OCP are listed in Table 3. Here, especially the output constraints show that we need to achieve a full transition with at least $20\frac{m}{s}$ as the final velocity and a flight condition close to the straight level horizontal flight.
Overall, the OCP in Eq. 6 is optimized with respect to the following cost:

$$J = t_f \tag{11}$$

Thus, we are seeking a time optimal transition within the robust OC framework.

4.2 Optimization Results

This section discusses the results for the robust OC of the VTOL with the model introduced in subsection 4.1. First of all, the sidewards wind velocity (i.e., the wind from the east direction) is modeled as the uncertainty with a UNIFORM distribution in the interval $[-5;+5]\frac{m}{s}$. In the scenario of the VTOL transitioning this is a meaningful uncertainty as the influence of the sidewards wind is crucial for a stable transition.
Additionally, seven control authority factors are

Table 2: States, controls, and outputs for the VTOL optimization model.

Description	Symbol	Lower Bound	Upper Bound	Scaling	Offset
States					
x Position	x	$-\infty$	$+\infty$	1	$0m$
y Position	y	$-\infty$	$+\infty$	1	$0m$
Altitude	z	$0m$	$+\infty$	1	$0m$
Quaternion 0	q_0	-1	$+1$	1	0
Quaternion 1	q_1	-1	$+1$	1	0
Quaternion 2	q_2	-1	$+1$	1	0
Quaternion 3	q_3	-1	$+1$	1	0
Body x Velocity	u	$+10^{-7}\frac{m}{s}$	$+50\frac{m}{s}$	1	$0\frac{m}{s}$
Body y Velocity	v	$-35\frac{m}{s}$	$+35\frac{m}{s}$	1	$0\frac{m}{s}$
Body z Velocity	w	$-35\frac{m}{s}$	$+35\frac{m}{s}$	1	$0\frac{m}{s}$
Body x Rotation	p	$-20\frac{°}{s}$	$+20\frac{°}{s}$	1	$0\frac{°}{s}$
Body y Rotation	q	$-20\frac{°}{s}$	$+20\frac{°}{s}$	1	$0\frac{°}{s}$
Body z Rotation	r	$-20\frac{°}{s}$	$+20\frac{°}{s}$	1	$0\frac{°}{s}$
Controls					
Rotor 1 Speed (Left)	ω_1	$+0\frac{rad}{s}$	$+1570.8\frac{rad}{s}$	1	$+750\frac{rad}{s}$
Rotor 2 Speed (Right)	ω_2	$+0\frac{rad}{s}$	$+1570.8\frac{rad}{s}$	1	$+750\frac{rad}{s}$
Rotor 3 Speed (Front)	ω_3	$+0\frac{rad}{s}$	$+1570.8\frac{rad}{s}$	1	$+750\frac{rad}{s}$
Rotor 4 Speed (Rear)	ω_4	$+0\frac{rad}{s}$	$+1570.8\frac{rad}{s}$	1	$+750\frac{rad}{s}$
Elevator	η	$-25°$	$+25°$	1	$0°$
Rotor 1 Pitch	δ_1	$-30°$	$+120°$	1	$+43°$
Rotor 2 Pitch	δ_2	$-30°$	$+120°$	1	$+43°$
Outputs					
Kinematic Velocity	V_K	$+10^{-7}\frac{m}{s}$	$+25\frac{m}{s}$	1	$+10\frac{m}{s}$
Kinematic Climb	γ_K	$-85°$	$+85°$	1	$0°$
Funnel Distance	d_F	$+0.1m$	$+\infty$	1	$0m$
Roll Angle	ϕ	$-30°$	$+30°$	1	$0°$
Yaw Angle	ψ	$-\infty$	$+\infty$	1	$0°$

Table 3: Initial and final state and output conditions for the VTOL OC.

Symbol	Initial Value Bounds	Final Value Bounds
States		
x	$0m$	free
y	$0m$	free
z	$+0.1m$	$\geq +4.5m$
q_0	$+1$	free
q_1	0	free
q_2	0	free
q_3	0	free
u	$+0.1\frac{m}{s}$	free
v	$0\frac{m}{s}$	$0\frac{m}{s}$
w	$0\frac{m}{s}$	free
p	$0\frac{°}{s}$	$0\frac{°}{s}$
q	$0\frac{°}{s}$	$0\frac{°}{s}$
r	$0\frac{°}{s}$	$0\frac{°}{s}$
Outputs		
V_K	auto set	$\geq +20\frac{m}{s}$
γ_K	free	$[-0.5;+0.5]°$
ϕ	auto set	$0°$
ψ	auto set	$0°$

introduced and limited as follows:

$$\begin{aligned} k_{\omega_1} &\in [+0.9;+1.0], \quad k_{\omega_2} \in [+0.9;+1.0] \\ k_{\omega_3} &\in [+0.9;+1.0], \quad k_{\omega_4} \in [+0.9;+1.0] \\ k_{\eta} &\in [+0.7;+1.0], \quad k_{\delta_1} \in [+0.6;+1.0] \\ k_{\delta_2} &\in [+0.6;+1.0] \end{aligned} \tag{12}$$

These factors are multiplied with their control commands respectively (Table 2). Thus, if the factor is < 1, the commanded value is reduced and the control authority is limited. This shapes a different trajectory design and ultimately creates a robust trajectory.

Overall, the bi-level framework tries to optimize these parameters to create a trajectory that has a maximized mean funnel distance during the transition and escape.

The optimized values for the control authority parameters obtained from the bi-level OC framework for the VTOL transition optimization are as follows:

$$\begin{aligned} k_{\omega_1} &\approx 0.90002, \quad k_{\omega_2} \approx 0.98738 \\ k_{\omega_3} &\approx 0.99994, \quad k_{\omega_4} \approx 0.96472 \\ k_{\eta} &\approx 0.90088, \quad k_{\delta_1} \approx 0.90845 \\ k_{\delta_2} &\approx 0.77290 \end{aligned} \tag{13}$$

It is intersting to observe from the control effectiveness factors in Eq. 13 that the control effectiveness is not adapted symmetrically. This is based on the fact that the VTOL has a lateral offset of the center of gravity from the symmetric plane and therefore the reference point. This offset is to the right wing and leads to a necessity to control the VTOL asymmetrically. This asymmetry is then also seen in the control effectiveness factors.

Another interesting observation from Eq. 13 is the fact that the control effectiveness factor for the first rotor k_{ω_1} is close to the lower bound of the feasible domain (Eq. 12). As a consequence, a new optimization should reduce the bound value further to see if another optimal solution can be obtained. This behavior is also an issue of the proposed bi-level OC framework as the control effectiveness limits in Eq. 12 are unknown a priori.

Figure 4 depicts the transition trajectories of the VTOL to escape from the funnel for the non-robust (solid red) and the the robust (dashed green) case. It is observed that the non-robust trajectories takes a slightly longer trajectory, while it also is a more steep in the beginning and climbs to a higher altitude.

The positional state development over the transition maneuver time is given in Figure 5. The behavior of Figure 4 is again observed. The small lateral deviations are due to the center of gravity shift as mentioned before. It is also observed that the transition time is approximately $0.4s$ longer for the robust case.

Finally, Figure 6 depicts the mean value and the standard deviation of the funnel distance for the robust and the non-robust transition maneuver. It is observed that the robust maneuver stays well above the minimal distance separation of $+0.1m$ (Table 2), while the non-robust trajectory meats this limit (approximately at $0.7s$). Evidently, considering further model errors (e.g., unmodeled dynamics or uncertainties) this close proximity to the limit is not robust in the end.

It is also observed in Figure 6 that the standard deviation of the funnel distance is slightly larger for the robust trajectory. This is due to the slower transition and climb and therefore larger time interval of exposition to the uncertainty.

Additionally, there is a weighting of minimal transition time and maximal funnel distance by the control effectiveness parameters. As these parameters are assigned to each of the gPC OCP equally, different trajectories that either prioritize the final time or the funnel distance are calculated. This behavior and the limitation of its influence within the bi-level OC is subject to future research.

Nonetheless, the distance to the funnel considering this increased standard deviation is still large enough. For future studies an incorporation of the standard deviation in the upper level cost can be considered as well, such that both the funnel distance is maximized and the funnel distance standard deviation is minimized. This yields a trade-off based on the user's priorities.

5 Conclusion and Perspective

This study presented a robust OC framework using a bi-level setup. The framework combined DE optimization in an upper level with gradient based OC in multiple lower level OCP.

A distinct feature of the lower level is the calculation of uncertain representations of optimal trajectories. This gives the upper level the capability to optimize statistical moments and by this ultimately the capability to increase the robustness by shaping the trajectories.

The developed bi-level framework is applied to the optimization of the transition maneuver of a VTOL. It showed its applicability in aircraft OC scenarios. The results show that the algorithm is capable of calculating robust trajectories with respect to specified parameter uncertainties.

Future research should consider the development of gradient based updates for the upper level based on postoptimal OC and gPC sensitivities. This will increase the convergence speed of the bi-level framework.

Additionally, different parameter settings in the upper level, including time varying control authority factors, can be considered to improve the robust trajectory results.

6 Contact Author Email Address

patrick.piprek@tum.de

Acknowledgment

This research was supported by the Deutsche Forschungsgemeinschaft (DFG) through the TUM International Graduate School of Science and Engineering (IGSSE).

The authors wish to thank Florian Wachter who contributed the visualization and Michael Krenmayr and Venkata Sravan Akkinapalli who contributed the initial simulation model. Additionally, the authors wish to thank Johannes Diepolder and Benedikt Grueter for the support with optimal control related questions.

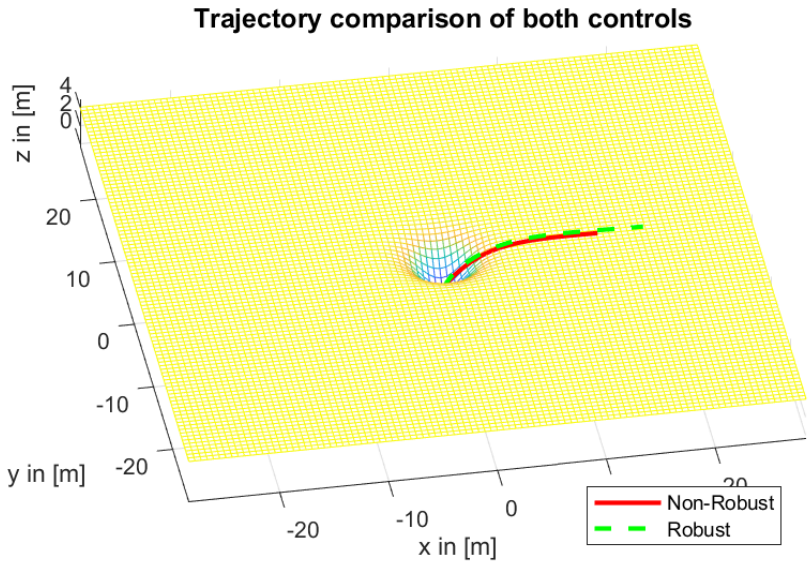

Fig. 4 : View on robust (dashed-green) and non-robust (solid red) VTOL transition trajectory with escape from funnel.

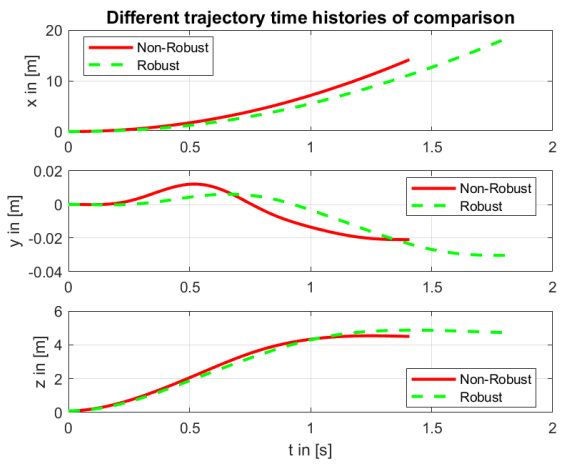

Fig. 5 : Robust (dashed-green) and non-robust (solid red) VTOL positions during the transition maneuver over time.

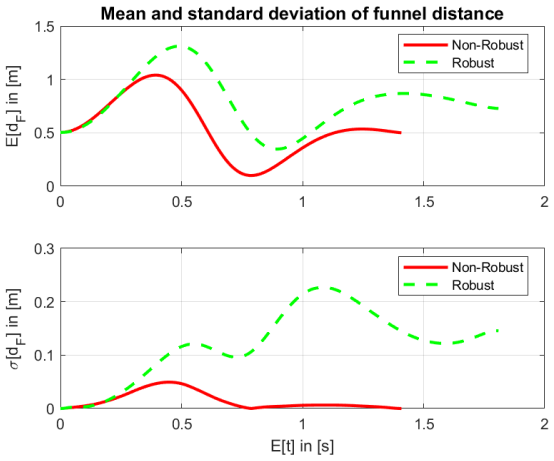

Fig. 6 : Mean and standard deviation of the funnel distance over the transition maneuver time for robust (dashed-green) and non-robust (solid red) transition.

Copyright Statement

References

[1] J. García-Heras, M. Soler, and F. J. Sáez, "A comparison of optimal control methods for minimum fuel cruise at constant altitude and course with fixed arrival time," *Procedia Engineering*, vol. 80, pp. 231–244, 2014.

[2] I. M. Ross and M. Karpenko, "A review of pseudospectral optimal control: From theory to flight," *Annual Reviews in Control*, vol. 36, no. 2, pp. 182–197, 2012.

[3] D. Xiu and G. E. Karniadakis, "The wiener-askey polynomial chaos for stochastic differential equations," *SIAM Journal on Scientific Computing*, vol. 24, no. 2, pp. 619–644, 2002.

[4] G. Cottrill, "Hybrid solution of stochastic optimal control problems using gauss pseudospectral method and generalized polynomial chaos algorithms," Dissertation, Air Force Institute of Technology, Ohio, 2012.

[5] T. C. Flanzer, "Robust trajectory optimization and control of a dynamic soaring unmanned aerial vehicle," Ph.D. dissertation, Stanford University, 2012.

[6] Y. Matsuno and T. Tsuchiya, "Stochastic 4d trajectory optimization for aircraft conflict resolution," in *IEEE Aerospace Conference, 2014*. Piscataway, NJ: IEEE, 2014, pp. 1–10.

[7] X. Li, P. B. Nair, Z. Zhang, L. Gao, and C. Gao, "Aircraft robust trajectory optimization using nonintrusive polynomial chaos," *Journal of Aircraft*, vol. 51, no. 5, pp. 1592–1603, 2014.

[8] K. Okamoto and T. Tsuchiya, "Optimal aircraft control in stochastic severe weather conditions," *Journal of Guidance, Control, and Dynamics*, vol. 39, no. 1, pp. 77–85, 2016.

[9] M. Richter and F. Holzapfel, "Robust noise optimal approach trajectories," *AIAA Guidance, Navigation, and Control (GNC) Conference, Boston*.

[10] N. Wiener, "The homogeneous chaos," *American Journal of Mathematics*, vol. 60, no. 4, p. 897, 1938.

[11] D. Xiu, "Fast numerical methods for stochastic computations - a review," *Communications in Computational Physics*, vol. 5, no. 2-4, pp. 242–272, 2009.

[12] T. Arens, F. Hettlich, Karpfinger Christian, U. Kockelkorn, K. Lichtenegger, and H. Stachel, Eds., *Mathematik*. Heidelberg: Spektrum, Akad. Verl., 2010.

[13] J. T. Betts, *Practical methods for optimal control and estimation using nonlinear programming*, 2nd ed., ser. Advances in design and control. Philadelphia, Pa: Society for Industrial and Applied Mathematics (SIAM 3600 Market Street Floor 6 Philadelphia PA 19104), 2010.

[14] M. Rieck, M. Bittner, B. Grüter, and J. Diepolder, "Falcon.m user guide," 2016. [Online]. Available: www.falcon-m.com

[15] A. Wächter and L. T. Biegler, "On the implementation of an interior-point filter line-search algorithm for large-scale nonlinear programming," *Mathematical Programming*, vol. 106, no. 1, pp. 25–57, 2006.

[16] B. L. Stevens and F. L. Lewis, *Aircraft control and simulation*, 2nd ed. Hoboken, NJ: Wiley, 2003. [Online]. Available: http://www.loc.gov/catdir/bios/wiley046/2003043250.html

[17] V. Feoktistov, *Differential Evolution: In Search of Solutions*. New York: Springer, 2006.

[18] International Organization for Standardization, "Standard atmosphere," Geneva, Switzerland, 05-1975. [Online]. Available: https://www.iso.org/standard/7472.html